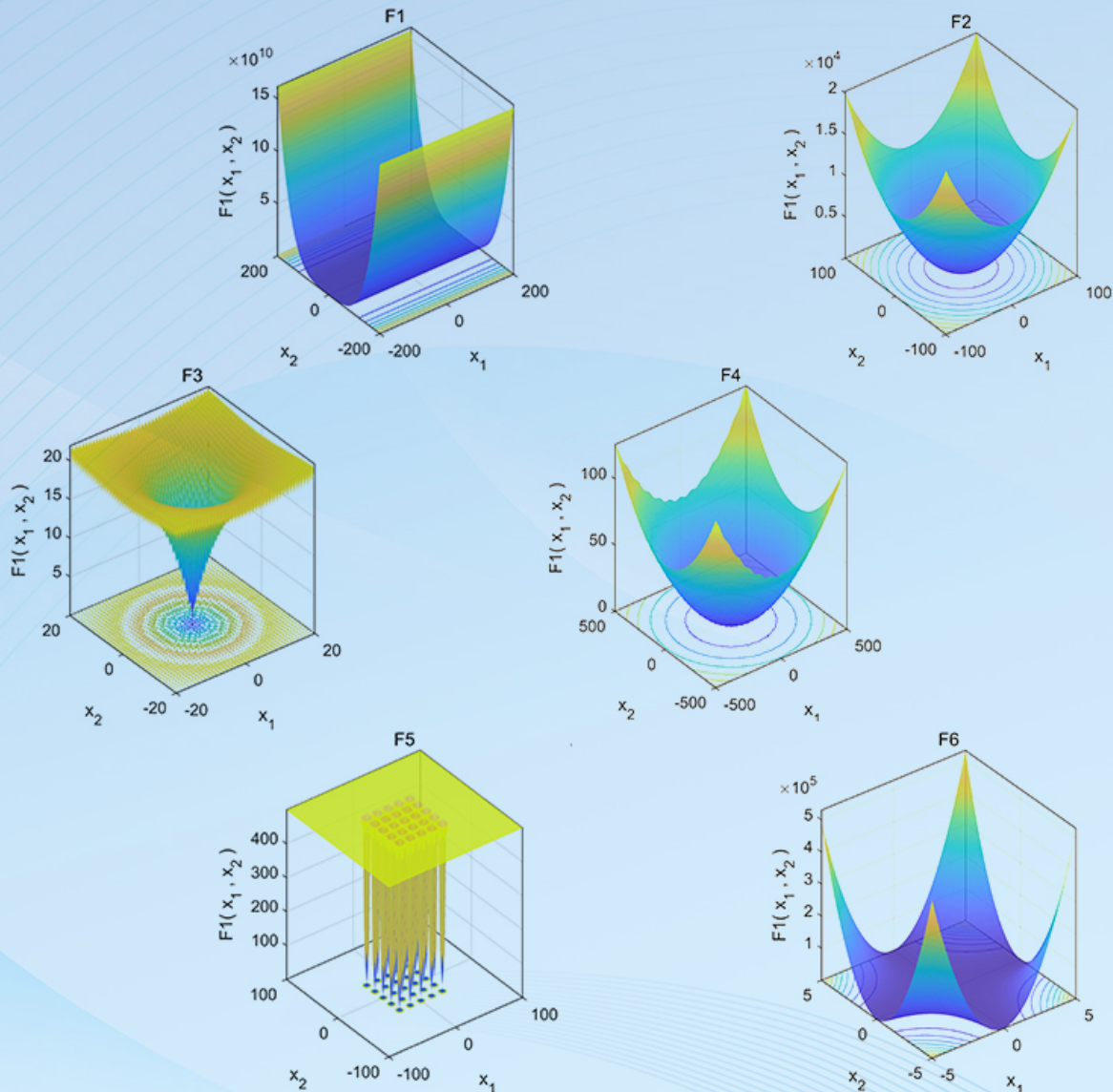# INTELLIGENCE & ROBOTICS

Time-optimal trajectory planning for a six-degree-of-freedom manipulator: a method integrating RRT and chaotic PSO

Zuoxun Wang*, Chuanzhe Pang, Jinxue Sui, Guojian Zhao, Wangyao Wu, Liteng Xu

Research Article

Dynamic event-triggered integral non-singular terminal sliding mode tracking of unmanned surface vehicle via an event-triggered extended state observer and adaptive neural network

Xingmin Wang[1], Ruixue Liu[1], Aleksander Sladkowski[2], Qian Li[1], Ru Jiang[1]

[1]Institute of Automation, Qilu University of Technology (Shandong Academy of Sciences), Shandong Provincial Key Laboratory of Robot and Manufacturing Automation Technology, Jinan 250014, Shandong, China.
[2]Faculty of Transport and Aviation Engineering, Silesian University of Technology, Gliwice 44100, Poland.

Correspondence to: Dr. Ru Jiang, Institute of Automation, Qilu University of Technology (Shandong Academy of Sciences), Shandong Provincial Key Laboratory of Robot and Manufacturing Automation Technology, No. 19, Keyuan Road, Lixia District, Jinan 250014, Shandong, China. E-mail: jiangr_sdas@163.com

Abstract

This paper presents a novel trajectory tracking controller for an underactuated unmanned surface vehicle (USV). The controller incorporates an event-triggered extended state observer (ETESO), a minimum learning parameter neural network, an integral non-singular terminal sliding mode (INTSM) control strategy, and a dynamic event-triggered mechanism (DETM). Firstly, an ETESO is developed to estimate unmeasurable velocities and lumped disturbances, differentiating it from most existing extended state observers without the necessity for real-time output measurements. To further alleviate the communication burden and minimize actuator wear, a DETM with an adjustable threshold is introduced. In contrast to traditional event-triggered methods, which employ fixed threshold parameters, this mechanism allows for online adaptive updates of the triggering thresholds, thereby enhancing resource efficiency. Additionally, an INTSM is designed to ensure rapid convergence of the position and velocity errors of the USV. To effectively counteract external disturbances and internal modeling uncertainties, a minimum learning parameter (MLP) neural network algorithm is implemented to approximate and compensate for these uncertainties. Finally, using Lyapunov's theory, it is demonstrated that all signals within the closed-loop tracking control system remain bounded. Simulation results are given to illustrate the effectiveness of theoretical results.

1. INTRODUCTION

The ocean is the largest and most complex ecosystem on Earth, covering approximately 71% of the planet's surface and harboring rich biodiversity and resources. In recent years, the rapid growth of the global population has led to a sharp increase in energy consumption, which in turn has intensified environmental pollution, posing a continuous threat to the living conditions of humans on land[1]. Ocean exploration is not only an important area of scientific research but also a key factor in achieving sustainable development for humanity. At the same time, with increasing attention on maritime rights by various countries, the ocean has become a focal point of international competition[2]. Unmanned surface vehicles (USVs) have garnered significant interest from the control science community[3]. This is mainly due to their advantages in a simple control structure and low manufacturing cost[4]. In terms of application, USVs have been employed in several contexts, including seabed resource extraction, bathymetry, marine search and rescue, oceanographic surveys, and sampling and patrolling[5]. However, the complexity of the marine environment, the unmodeled dynamics in the mathematical models of the USV, and the inability to measure the speed of USV in real-world ocean conditions can lead to a degradation of the maneuvering performance of the USV, potentially causing instability in system performance. Moreover, the real-time transmission of command signals from the controller to the actuators can lead to unnecessary communication burdens and excessive wear on the actuators[6]. Given these challenges, further research into USVs and their integration into offshore engineering is crucial.

Typically, the data exchange of the USV is facilitated through wireless communication networks. This involves connecting system components, such as sensors, controllers, filters, and actuators, through the communication network, with controllers typically situated in remote motherships or land-based stations[7]. Therefore, it is paramount to reduce the computational cost and conserve communication resources to achieve adequate control of the USV. In light of the circumstances above, event-triggered control has garnered increasing attention in recent years, as evidenced by the work of[8]. Jiang *et al.* presented a method for addressing the adverse effects of denial of service (DoS) attacks by incorporating the phenomenon of signal non-transmission into the event-triggered interval[9]. Zhou *et al.* proposed an event-triggered control mechanism scheme based on dynamic surface control and adaptive dynamic programming[10]. This approach ensures that tracking the reference trajectory effectively saves computation and reduces the number of controller executions. However, the event-triggered thresholds in the above studies are static, which imposes rigid communication at the expense of performance. In order to further reduce the computational cost and save communication resources, Girard and Antoine (2014) presented a dynamic triggering mechanism for event-triggered control[11]. Subsequently, dynamic event-triggered mechanisms (DETM) have been widely applied in the field of control. For example, Cao *et al.* combined network-induced errors and relative threshold strategies to establish two new DETM and dynamic rules for threshold parameters, reducing communication between the controller and the actuator[12]. He *et al.* proposed a distributed dynamic event-triggered strategy, introducing an auxiliary parameter for each agent to dynamically adjust its threshold[13]. Wang and Chang proposed a new DETM[14]. By analyzing data in real time, the event-triggering parameters are adjusted to ensure better triggering performance. Compared with the traditional static event-triggered control, dynamic event triggering has a longer time interval. However, there is currently no trajectory tracking control algorithm for USVs based on DETM. Therefore, researching trajectory tracking control for USVs based on DETM is of significant importance.

The theory of sliding mode control was mainly developed in the early 1990s[15]. In recent years, sliding mode variable structure control has been widely used in the USV control field because of its strong robustness, fast response and simple implementation[16,17]. In order to reduce the jitter of the system and improve the ex-

emplary reading of the control system, Liu *et al.* utilized super-twisting sliding mode control to design the system [18]. Yu *et al.* employed an integral form of the sliding mode surface for the control of the USV [19]. This approach effectively reduces the system's steady-state error and enhances its steady-state performance. In addition, Zhang *et al.* used a terminal sliding mode surface to achieve the convergence of the control error of the USV system in a finite time [20]. Although this terminal sliding surface can make the system state converge in finite time, it may make the system exist at a singular point of zero. Based on those mentioned above, this paper employs an integral form of non-singular terminal sliding mode surface for trajectory tracking control of the USV; That is, it can make the system error converge in finite time without a singular point and eliminate the system's steady-state error.

Many methods have been used to estimate disturbances and interferences in the control of USVs. Sun *et al.* studied the optimal coverage control problem for multiple USVs under time-varying disturbances [21]. A disturbance vector observer was designed to approximate the unknown time-varying disturbances to address this issue. In the study of Han *et al.*, a nonlinear version of the Kalman filter-based active modeling method was proposed to provide online estimates of the unstructured model to eliminate the errors due to the structural inaccuracies between the quasi-linear parameter-varying (qLPV)-structured model and the natural system [22]. Chen *et al.* proposed a disturbance-observer-based sliding mode control design to achieve good tracking performance, where the observer estimated and compensated for the modeling uncertainties and external disturbance [23]. In the study of Chen *et al.*, an adaptive sliding mode control design for nonlinear USVs is proposed, incorporating a radial basis function neural network to approximate system modeling uncertainty and a disturbance observer to estimate external unknown disturbances [24]. However, radial basis function neural network algorithms require online adjustment of the ownership vector of the network, which increases the computational effort. Therefore, the minimum learning parameter (MLP) neural network algorithm can solve the problem effectively. Most of the above studies assume that the speed of unmanned vessels is measurable and controllers are directly designed based on this assumption. However, the actual speed of marine vessels during navigation is not measurable. Therefore, it is necessary to estimate the state variables using available information (inputs and outputs) through models. Using observer-based feedback control is a very important strategy. Typically, an observer is added to establish a simulation system with the same dynamic equations as the actual system, thereby enabling state estimation, system performance analysis, and control design [25].

Based on the information provided, this paper puts forward an integral non-singular terminal sliding mode (INTSM) trajectory tracking control algorithm. An event-triggered extended state observer (ETESO) is developed to estimate the velocity and utilizes an MLP neural network algorithm to estimate the internal and external disturbances of the USV. Furthermore, dynamic event triggers are incorporated into the control channel to conserve communication resources while tracking a specified trajectory. The primary contributions of this paper compared to existing research results are as follows:

(1) firstly, this paper introduces a DETM with adjustable thresholds into the USV's control input. In contrast to the existing event-triggered mechanisms widely used in USV trajectory tracking control [26,27], which have fixed threshold parameters for triggering results, the mechanism employed in this study can adaptively update the triggering thresholds online, thereby conserving communication resources more effectively. Additionally, to further save communication resources, an event-triggered mechanism has also been incorporated into the extended state observer;

(2) compared to the traditional sliding mode surfaces used for trajectory tracking control of the USV in ref. [28,29], the INTSM surface employed in this paper not only ensures that the tracking error of the USV converges within a finite time but also reduces the steady-state error of the system;

(3) in relation to ref. [30,31], which uses radial basis function neural networks to directly approximate USV's

modeling uncertainties and external disturbances, this paper further employs the MLP technique to compress the weights of the neural network. Replacing the online learning of all weight vectors with single-parameter online learning reduces the amount of computation required to estimate and compensate for external disturbances.

2. PROBLEM DESCRIPTION AND PRELIMINARY PREPARATION

2.1. Model of USV

The mathematical modeling of USVs is essential for analyzing their motion dynamics. In recent studies addressing trajectory tracking control for underactuated vessels, the Fossen model is predominantly employed, where the longitudinal thrust and steering torque of the USV serve as control outputs to regulate its movement[32]. Following this, the kinematic and dynamic models of the USV can be represented mathematically as follows:

$$\dot{\eta} = R(\psi) v, \quad M\ddot{\eta} + C_0\dot{\eta} + D_0\dot{\eta} = R\tau + \Delta f + \tau_w. \tag{1}$$

The variables are defined as follows: $\eta = [x, y, \psi]^T$ represents the surge, sway, and yaw angle of the ship in the inertial frame; $v = [u, v, r]^T$ represents the velocity vector of the ship in the body-fixed frame; $R(\psi)$ is the transformation matrix between the inertial frame and the body-fixed frame, and it satisfies $R^{-1}(\psi) = R^T(\psi)$; M is the inertia matrix of the ship and satisfies $M = M^T > 0$; $C(v)$ is the Coriolis and centripetal matrix and satisfies $C(v) = -C(v)^T$; D is the damping matrix; $\tau = [\tau_u, 0, \tau_r]^T$ is the control force and moment vector for the underactuated ship, where τ_u and τ_r represent the longitudinal thrust and the steering moment, respectively. For underactuated ships, there is no lateral thruster, so $\tau_v = 0$; $\tau_w = [\tau_{wu}, 0, \tau_{wr}]^T$ denotes the unknown environmental time-varying interference in the body-fixed frame, where τ_{wu} is the environmental interference forces of the ship in the longitudinal directions, and τ_{wr} is the interference force of the ship in the yaw direction. The expressions for $R(\psi)$, M, $C(v)$, and D are given by:

$$R(\psi) = \begin{bmatrix} \cos\psi & -\sin\psi & 0 \\ \sin\psi & \cos\psi & 0 \\ 0 & 0 & 1 \end{bmatrix}, M = \begin{bmatrix} m_{11} & 0 & 0 \\ 0 & m_{22} & 0 \\ 0 & 0 & m_{33} \end{bmatrix}$$

$$C(v) = \begin{bmatrix} 0 & 0 & -m_{22}v \\ 0 & 0 & m_{11}u \\ m_{22}v & -m_{11}u & 0 \end{bmatrix}, \quad D = \begin{bmatrix} d_{11} & 0 & 0 \\ 0 & d_{22} & 0 \\ 0 & 0 & d_{33} \end{bmatrix}$$

Moreover, the parameters are defined as follows: $m_{11} = m - X_{\dot{u}}, m_{22} = m - Y_{\dot{v}}, m_{33} = I_z - N_{\dot{r}}, d_{11} = -X_u$, $d_{22} = -Y_v$, $d_{33} = -N_r$. m represents the mass of the underactuated ship, I_z is the moment of inertia, and other parameters such as $X_i = \partial X/\partial \dot{u}$ are hydrodynamic derivatives. These symbols were standardized by the Society of Naval Architects and Marine Engineers (SNAME) in 1950, and will not be elaborated here. The mathematical model of the USV can also be written in the following form:

$$\begin{cases} \dot{x} = u\cos(\psi) - v\sin(\psi) \\ \dot{y} = u\sin(\psi) + v\cos(\psi) \\ \dot{\psi} = r \\ \dot{u} = \dfrac{1}{m_{11}}(m_{22}vr - d_{11}u + \Delta f_u + \tau_u + \tau_{wu}) \\ \dot{v} = \dfrac{1}{m_{22}}(-m_{11}ur - d_{22}v + \Delta f_v + \tau_{wv}) \\ \dot{r} = \dfrac{1}{m_{33}}((m_{11} - m_{22})uv - d_{33}r + \Delta f_r + \tau_r + \tau_{wr}) \end{cases} \tag{2}$$

2.2. Design of ETESO

In this section, ETESO is designed to obtain accurate estimates of velocities with fewer communication resources. According to the USV mathematical model in Equation (1), the composite dynamics model of the system is given as:

$$\ddot{\eta} = \mathbf{R}(\psi)\dot{v} + \dot{\mathbf{R}}(\psi)v = \mathbf{R}(\psi)\mathbf{M}^{-1}[-\mathbf{C}(v) - \mathbf{D}v - \tau_w - \Delta\mathbf{f}] + \dot{\mathbf{R}}(\psi)\mathbf{v} + \mathbf{R}(\psi)\mathbf{M}^{-1}\tau = \chi + \mathbf{R}(\psi)\mathbf{M}^{-1}\tau \quad .$$

(3)

We define $\mathbf{x}_1 = \eta$, $\mathbf{x}_2 = \dot{\eta}$. Consequently, the dynamics model of the USV can be expressed as:

$$\begin{cases} \dot{\mathbf{x}}_1 = \mathbf{x}_2 \\ \dot{\mathbf{x}}_2 = \chi + \mathbf{R}(\psi)\mathbf{M}^{-1}\tau \end{cases} ,$$

(4)

where $\chi = \mathbf{R}(\psi)\mathbf{M}^{-1}[-\mathbf{C}(\mathbf{v}) - \mathbf{D}v - \tau_w - \Delta\mathbf{f}] + \dot{\mathbf{R}}(\psi)v$ represents the lumped uncertainty, which includes unmodeled dynamics and external disturbances.

To design ETESO, we introduce Assumption 1, which is often used in the control of the USV [33].

Assumption 1 [34] The composite disturbance vector $\tau_w = [\tau_{wu}, 0, \tau_{wr}]$ is time-varying and unknown, with its Euclidean norm bounded by a constant, i.e., $\| \tau_w \| < \bar{\tau}_w$, where $\bar{\tau}_w$ is a constant. Additionally, the lumped uncertainty χ satisfies $\| \dot{\chi} \| \le H$, where $H > 0$ is an unknown bounded constant.

The following ETESO is designed

$$\begin{cases} \dot{\hat{\mathbf{x}}}_1 = \hat{\mathbf{x}}_2 + \varepsilon_e g_1\left(\frac{\xi(\mathbf{t}) - \hat{\mathbf{x}}_1(t)}{\varepsilon_e^2}\right) \\ \dot{\hat{\mathbf{x}}}_2 = \hat{\mathbf{x}}_3 + g_2\left(\frac{\xi(\mathbf{t}) - \hat{\mathbf{x}}_1(t)}{\varepsilon_e^2}\right) + R(\psi)M^{-1}\tau \\ \dot{\chi} = \varepsilon_e^{-1} g_3\left(\frac{\xi(\mathbf{t}) - \hat{\mathbf{x}}_1(t)}{\varepsilon_e^2}\right) \end{cases} ,$$

(5)

where $\hat{\mathbf{x}}_1$, $\hat{\mathbf{x}}_2$ and χ are estimate of $\mathbf{x}_1$, $\mathbf{x}_1$ and χ, respectively. The parameter ε_e is a high-gain parameter to be determined. The functions $g_i(*), i = 1, 2, 3$ are defined as follows: $g_1(\vartheta) = a_1\vartheta + \varphi(\vartheta)$, $g_j(\vartheta) = a_j\vartheta$, $j = 2, 3$,

are constants to be chosen to ensure that the matrix $N = \begin{bmatrix} -a_1 & 1 & 0 \\ -a_2 & 0 & 1 \\ -a_3 & 0 & 0 \end{bmatrix}$ is Hurwitz, and $\varphi(\vartheta)$ is defined as

$\varphi(\vartheta) = \begin{cases} \frac{1}{4}sign(\vartheta), & if|\vartheta| > \frac{\pi}{2} \\ \frac{1}{4}sin(\vartheta), & if|\vartheta| \le \frac{\pi}{2} \end{cases}$. where $\zeta(t)$ is the measurement output, which is defined as:

$$\zeta(t) = \begin{cases} \eta(t_{o,k}), if \Gamma_1 \le 0, \\ \eta(t), \quad otherwise, \end{cases}$$

(6)

with an event-triggered condition given by $\Gamma_1 = \sum_{i=1}^{3} L_i|\sigma(t)| - \overline{B}\varepsilon_e$, where $\overline{B}$ is a positive constant to be determined, and $L_i > 0$ is a Lipschitz constant for $g_i(*)$. The $\sigma(t)$ is an sampled error defined as $\sigma(t) = \frac{\eta(t_{o,k}) - \eta(t)}{\varepsilon_e^2}$, for $t \in [t_{o,k}, t_{o,k+1})$. Here, $t_{o,k}$ denotes the triggered instant, which depends on condition 6.

Lemma 1 [35] For any $\ell > 0$ and $a \in \mathbb{R}$, the following inequality holds:

$$0 \le | a | - a \tanh(\frac{a}{\ell}) \le \aleph a.$$

(7)

Given that $\aleph = e^{-(1+\aleph)}$, we take $\aleph = 0.2785$.

Lemma 2 [36] For a given unknown continuous function $f(\mathbf{x}):\mathfrak{R}^m \to \mathfrak{R}$, it can be approximated over a compact set $\Omega_x \subset \mathfrak{R}^m$ with the following radial basis function neural network:

$$f = W^{*T}h(z) + \varepsilon$$

(8)

where $W^{*T} = [W_1^*, W_1^*, , W_k^*]^T$ is the ideal weight vector with k being the number of NN nodes and matrix $z = [u, v, r]^\tau$ represents the input signals of radial basis function neural network. ε represents the estimated error of neural network with the upper bound $|\varepsilon| \leq \varepsilon^*$, where ε^* is an unknown positive constant. The basis function $h(x) = [h_1(x), h_2(x), ..., h_n(x)]^\tau$ is chosen as the Gaussian function, that is

$$h_j(x) = \exp\left[-\frac{\|x - c_j\|^2}{2b_j^2}\right], (j = 1, \cdots, n)$$ (9)

where $b_j > 0$ and $c_j = [c_1, c_2, \cdots, c_m]^T \in \mathbf{R}^m$ are the center of the receptive field and the width of the Gaussian function. Formally, the optimal weight vector W^* is computed as:

$$W^* = arg \min_{\hat{\gamma} \in \mathbb{R}^k} \left\{ sup \left| f(x) - \hat{W}^T S(x) \right| \right\}$$ (10)

where $\hat{W}$ is the estimate of W^*.

Define $\tilde{W} = W^* - \hat{W}$, then

$$\tilde{f} = f - \hat{f} = W^{*T} h(z) + \varepsilon - \hat{W}^T h(z) = \tilde{W}^T h(z) + \varepsilon$$ (11)

Lemma 3 [37] Consider a nonlinearsystem $\dot{\mathbf{X}} = f(\mathbf{X}(t)), \mathbf{X} \in \mathfrak{R}$, if there exists a continuous and positive definite Lyapunov function $V(\mathbf{X})$ satisfying $k_1(\|\mathbf{X}\|) \leq V(\mathbf{X}) \leq k_2(\|\mathbf{X}\|)$ such that $\dot{V} \leq -lV + Q$, where k_1, k_2 are class κ functions and l, Q are positive constants, and then the solution $\mathbf{X}(t)$ is ultimately uniformly bounded.

3. TRAJECTORY TRACKING CONTROLLER DESIGN
In this section, we will design an INTSM controller to effectively track the trajectory of the USV. The complete design procedure will be elaborated upon in the following subsections.

3.1. Virtual control design
For future use, we will define the following tracking errors:

$$\begin{bmatrix} x_e \\ y_e \\ \psi_e \end{bmatrix} = J^{\mathrm{T}}(\psi) \begin{bmatrix} x_d - x \\ y_d - y \\ \psi_d - \psi \end{bmatrix},$$ (12)

where (x, y) denotes the position of the USV in the earth - fixed frame, , and ψ represents the vessel's yaw angle. The terms x_d, y_d, ψ_e denote the longitudinal position error, transverse position error, and heading angle error, respectively. Additionally, $z_e = \sqrt{x_e^2 + y_e^2}$, where x_e and y_e represent the vertical and horizontal position errors. These errors correspond to the horizontal and vertical coordinates of the reference trajectory. The expected course can be given as:

$$\psi_d = \begin{cases} \arctan\left(\frac{\dot{y}_d}{\dot{x}_d}\right), z_e = 0 \\ 0.5\left[1 - \text{sgn}(x_e)\right]\text{sgn}(y_e)\pi + \arctan\left(\frac{y_e}{x_e}\right), \text{other} \end{cases}.$$ (13)

In Figure 1, the coordinate system OXY represents the inertial reference frame, with point O as the initial position. The OX axis points due north, while the OY is due east. Point Ob is defined as the midpoint between the bow and stern of the USV. The vector $o_b x_b$ extends toward the bow along the USV's midline, and the vector $obyb$ is directed along the port side of the USV. Additionally, line segment AB represents the reference trajectory.

According to the relationships depicted in Figure 1, the variables x_e, y_e and z_e can be expressed as:

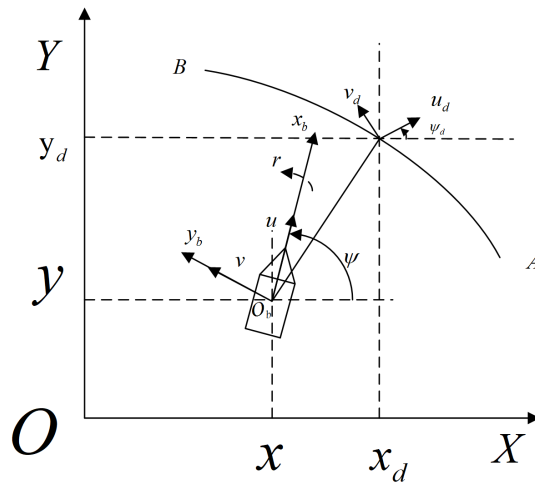$$x_e = z_e \cos \psi_d \qquad y_e = z_e \sin \psi_d.$$ (14)

Figure 1. Basic schematic diagram of USV trajectory tracking. USV: Unmanned surface vehicle.

Taking the time derivative of the variables z_e and ψ_e, along with utilizing Equations (2) and (14), we can derive

$$\begin{aligned} \dot{z}_e &= \dot{x}_d \cos \psi_d + \dot{y}_d \sin \psi_d - u \cos \psi_e - v \sin \psi_e \\ \dot{\psi}_e &= \dot{\psi}_d - r \end{aligned}. \tag{15}$$

Design the virtual control functions α_u and α_r as follows:

$$\alpha_u = \cos^{-1}(\psi_e) \left[k_{ze1} z_e + k_{ze2} \text{sgn}^\delta(z_e) \right] + \dot{x}_d \cos(\psi_d) + \dot{y}_d \sin(\psi_d) - v \sin(\psi_e), \tag{16}$$

$$\alpha_r = k_{\psi e1} \psi_e + k_{\psi e2} \text{sgn}^\delta(\psi_e) + \dot{\psi}_d, \tag{17}$$

where $k_{ze1} > 0, k_{ze2} > 0, k_{\psi e1} > 0, k_{\psi e2} > 0, 0.5 \leq \delta < 1$ are the design parameters.

Note that when $\psi_e = \pm \frac{\pi}{2}$, α_u becomes undefined. Therefore, in actual engineering, the first assumption is that condition $|\psi_e| < \frac{\pi}{2}$ holds, and the assumption is guaranteed by the transformation of[38]

$$\psi_e = \begin{cases} \psi_e - \pi, & \psi_e \geq 0.5\pi \\ \psi_e, & -0.5\pi < \psi_e < 0.5\pi \\ \psi_e + \pi, & \psi_e \leq -0.5\pi \end{cases} \tag{18}$$

3.2. Design of INTSM controller

To prevent dimensional explosion, we introduce the following first-order filter.

$$\mu \dot{\gamma} + \gamma = \alpha \quad \gamma(0) = \alpha(0), \tag{19}$$

where γ is first-order filter and μ denotes the time constant.

Define the longitudinal error and the yaw velocity error as:

$$e_u = u - \gamma_u, e_r = r - \gamma_r. \tag{20}$$

Introduction of an INTSM surface for longitudinal error and yaw velocity error:

$$S_i = \lambda_i \int_0^t sig^{r_i}(e_i) d\tau + \beta_i e_i, i = u, r \tag{21}$$

given that λ_i, β_i and $r_i > 1$ are designed constants, we proceed to differentiate S_i to obtain

$$\dot{S}_i = \lambda_i sig^{r_i}(e_i) + \beta_i \dot{e}_i, i = u, r \quad . \tag{22}$$

The surge motion control law τ_u and yaw motion control law τ_r can be designed as:

$$\tau_u = m_{11}\dot{\gamma}_u - \hat{\tau}^*_{wu}tanh(S_u/\hat{\varepsilon}_u) - \triangle\hat{f}_u + d_{11}\hat{u} - m_{22}\hat{v}\hat{r} - \frac{m_{11}\lambda_u sig^{r_u}e_u}{\beta_u} - k_u tanh(S_u), \tag{23}$$

$$\tau_r = m_{33}\dot{\gamma}_r - \hat{\tau}^*_{wr}tanh(S_r/\varepsilon_r) - \triangle\hat{f}_r + d_{33}\hat{r} - (m_{11} - m_{22})\hat{u}\hat{v} - \frac{m_{33}\lambda_r sig^{r_r}e_r}{\beta_r} - k_r tanh(S_r), \tag{24}$$

where $\triangle\widehat{f_u} = \frac{1}{2}s_u\widehat{\phi}_u hh^T$ and $\triangle\widehat{f_r} = \frac{1}{2}s_r\widehat{\phi}_r hh^T$ represent the estimate of $\triangle f_u$ and $\triangle f_r$, respectively. The corresponding adaptive laws are given in

$$\dot{\hat{\phi}}_i = \hat{\lambda}_i \left(\frac{1}{2}s_i^2 h^T h - \kappa_u \hat{\phi}_i\right), i = u, v \tag{25}$$

The adaptive law for model uncertainty in the USV is defined as follows:

$$\dot{\hat{\tau}}^*_{Wi} = \gamma_i \left[S_i\psi(S_i) - \mu_i\left(\widehat{\tau}^*_{wi} - \tau^0_{wi}\right)\right], i = u, v \tag{26}$$

3.3. Dynamic event-triggered input scheme with ETESO

In this subsection, we present a dynamic event-triggered control scheme in the last step. First, we define $\hat{\tau} = \begin{bmatrix} \hat{\tau}_u & \hat{\tau}_r \end{bmatrix}^T$, the dynamic event-triggered control law $\hat{\tau}$ is given as:

$$\hat{\tau}(t) = \tau(t_j), \forall t \in [t_j, t_{j+1}), j \in \mathbb{N}. \tag{27}$$

It is evident that $\hat{\tau}(t)$ is updated only at triggering instants t_j, where $j \in \mathbb{N}$. We define the measurement error $z(t)$ as

$$z(t) = \hat{\tau}(t) - \tau(t), \forall t \in [t_j, t_{j+1}), j \in \mathbb{N}. \tag{28}$$

The DETM is designed as:

$$t_{j+1} = \inf_{t>t_j}\{t \in \mathbb{R}_{\geq 0}|\eta_i(t) + (k_i - 1)S_i^2 - Z_i^2 \leq 0\}, t_0 = 0, \tag{29}$$

where $\eta(t)$ is an internal dynamic variable satisfying

$$\dot{\eta} = -\chi\eta + (k_i - 1)S_i^2 - Z_i^2, \eta(0) = \eta_0. \tag{30}$$

It is evident that the inequality $-\eta_k(t) \leq (k_i - 1)S_i^2 - Z_i^2$ holds all the time. We will now demonstrate that $\eta_k(t) > 0$ is indeed true. Based on the definition of $Z(t)$ in Equation (28), we can conclude that $||Z(t)|| \leq ||Z(t^-)||$ for all $t \geq 0$. Then, the DETM (29) ensures that for all $t > 0$

$$\eta_i(t) + (k_i - 1)S_i^2 - Z_i^2 \geq 0 \tag{31}$$

from Equation (31), we have

$$(k_i - 1)S_i^2 - Z_i^2 \geq -\eta_i(t) \tag{32}$$

Combining Equations (30) and (32), it can be deduced that for all $t \geq 0$

$$\dot{\eta}(t) \geq -\chi\eta(t) - \eta(t), \eta(0) = \eta_0 > 0. \tag{33}$$

Then by the Comparison Lemma, we can obtain that for all $t \geq 0$

$$\eta(t) \geq \eta_0 e^{-(\chi+1)t} \geq 0. \tag{34}$$

4. STABILITY ANALYSIS

To prove the stability of ETESO, we introduce Assumption 2, which is often used to ensure the stability of the nominal system considered [39].

Assumption 2 [40] There exist two nonnegative definite functions $P(*)$ and $W(*) : \mathbb{R}^{n+1} \to \mathbb{R}$ satisfying

$$\lambda_1 ||\vartheta||^2 \le P(\vartheta) \le \lambda_2 ||\vartheta||^2, \lambda_3 ||\vartheta||^2 \le W(\vartheta) \le \lambda_4 ||\vartheta||^2, \tag{35}$$

$$\sum_{j=1}^{n} \frac{\partial P}{\partial \vartheta_j} (\vartheta_{j+1} - g_j(\vartheta_1)) - \frac{\partial P}{\partial \vartheta_{n+1}} g_{n+1}(\vartheta_1) \le -W(\vartheta), \tag{36}$$

$$\left\| \frac{\partial P}{\partial \vartheta} \right\| \le \beta ||\vartheta||, \tag{37}$$

where β and λ_i are positive constants, $i = 1, \ldots, 4$.

Theorem 1 Consider the closed-loop system comprising the underactuated USV dynamics given in Equation (2), subject to modeling uncertainty and external disturbances. This system satisfies Assumptions 2, utilizing the intermediate control laws specified in Equations (23) and (24), the triggering instants defined in Equation (29), the ETESO in Equation (5), the MLP neural network update laws in Equation (25), and the adaptive laws given in Equation (26). By selecting appropriate parameters, all error signals in the system converge quickly to an arbitrarily small vicinity of the origin, while also ensuring that the Zeno phenomenon is excluded.

Proof 1 From Equations (4) and (5), we have for $\tilde{x}_i$ and $t \in [t_k, t_{k+1})$

$$\begin{cases} \dot{\mathbf{e}}_i = \frac{1}{\varepsilon}(e_{i+1}(t) - g_i(e_1(t)) - \alpha_i(e_1(t) - \sigma(t))), i = 1, 2, \\ \dot{\mathbf{e}}_3 = \dot{\mathbf{x}}_3 - \frac{1}{\varepsilon}(g_3(e_1(t)) + \alpha_3(e_1(t) - \sigma(t))), \end{cases} \tag{38}$$

Considering a positive semidefinite function $V_0 = P(e)$, and $P(e)$ is given by $P(\vartheta) = \langle \tilde{P}\vartheta, \vartheta \rangle P(*) : \mathbb{R}^{n+1} \to \mathbb{R}$, the matrix $\tilde{P}$ is a positive definite one satisfying $\tilde{P}N + N^T \tilde{P} = -I$, and I is the identity matrix. Taking the derivative of V_0, we can compute its derivative, which yields:

$$\frac{d}{dt} V_0(t) = \sum_{i=1}^{3} \frac{\partial P}{\partial e_i} \dot{e}_i(t) = \frac{1}{\varepsilon} \sum_{i=1}^{2} \frac{\partial P}{\partial e_i} (e_{i+1}(t) - g_i(e_1)) - \frac{1}{\varepsilon} \frac{\partial P}{\partial e_3} g_3(e_1(t)) - \frac{1}{\varepsilon} \sum_{i=1}^{3} \frac{\partial P}{\partial e_i} \alpha_i(e_1(t), \sigma(t)) + \frac{\partial P_0}{\partial e_3} \dot{\mathbf{x}}_3. \tag{39}$$

From Equations (35) and (36) in Assumptions 2, we have

$$\dot{V}_0(t) \le -\frac{\lambda_3}{\varepsilon} ||e||^2 + \beta \dot{x}_3 ||e|| - \frac{1}{\varepsilon} \sum_{i=1}^{3} \frac{\partial P}{\partial e_i} \alpha_i(e_1(t), \sigma(t)). \tag{40}$$

considering the fact that the functions g_i are assumed to be Lipschitz with $Li > 0$, it follows

$$|\alpha_i(e_1, \sigma)| = |g_i(e_1 + \sigma) - g_i(e_1)| \le L_i |e_1 + \sigma - e_1| = L_i |\sigma|. \tag{41}$$

By combining Equation (6), it yields

$$-\frac{1}{\varepsilon} \sum_{i=1}^{n+1} \frac{\partial P}{\partial e_i} \alpha_i(e_1(t), \sigma(t)) \le \left(\frac{\varepsilon^{-\frac{1}{3}} ||e||^2}{2} + \frac{\varepsilon^{\frac{1}{3}}}{2} \right) \overline{B}\beta. \tag{42}$$

According to Young's inequality, it follows that $\beta \dot{x}_{n+1} ||e|| \le \frac{\beta}{2\varepsilon} \left(\varepsilon^{\frac{2}{3}} ||e||^2 + \varepsilon^{\frac{4}{3}} |\dot{x}_{n+1}|^2 \right)$. Then, from Assumption 2, we can get

$$\beta \dot{x}_{n+1} ||e|| \le \frac{\beta}{2\varepsilon} \left(\varepsilon^{\frac{2}{3}} ||e||^2 + \varepsilon^{\frac{4}{3}} M^2 \right). \tag{43}$$

Substituting Equations (42) and (43) into Equation (40), from Assumption 2, it yields:

$$\dot{V}_0(t) \le -\frac{2\lambda_3 - \beta\varepsilon^{\frac{2}{3}} - \beta\varepsilon^{\frac{2}{3}}\overline{B}}{\varepsilon\lambda_2}V_0 + \frac{\varepsilon^{\frac{1}{3}}}{2}\beta(M^2 + \overline{B}), \tag{44}$$

where we choose parameters such that $\frac{2\lambda_3 - \beta\varepsilon^{\frac{2}{3}} - \beta\varepsilon^{\frac{2}{3}}\overline{B}}{\varepsilon\lambda_2} > 0$. Next, consider

$$V_1 = \frac{m_{11}}{2\beta_u}S_u^2 + \frac{m_{33}}{2\beta_r}S_r^2 + \frac{1}{2\gamma_u}\tilde{\tau}_{wu}^{*~2} + \frac{1}{2\gamma_r}\tilde{\tau}_{wr}^{*~2} + \frac{1}{2\hat{\lambda}_u}\tilde{\phi}_u^2 + \frac{1}{2\hat{\lambda}_r}\tilde{\phi}_r^2 + \eta. \tag{45}$$

Taking the derivative of V_1 and substituting Equations (23)-(26) into it have:

$$\dot{V}_1 = -k_u S_u^2 - k_r S_r^2 + S_u\boldsymbol{\phi}_u^{*\mathrm{T}}\boldsymbol{h}(\boldsymbol{z}) + \xi_u S_u + \dot{\eta} - \frac{1}{2}S_u^2\hat{\phi}_u\boldsymbol{h}^{\mathrm{T}}\boldsymbol{h} + S_r\boldsymbol{\phi}_r^{*\mathrm{T}}\boldsymbol{h}(\boldsymbol{z}) + \xi_r S_r - \frac{1}{2}S_r^2\hat{\phi}_r\boldsymbol{h}^{\mathrm{T}}\boldsymbol{h}$$

$$+ \tau_{wu}^*\left(|S_u| - S_u\phi(S_u)\right) + \tau_{wr}^*\left(|S_r| - S_r\phi(S_r)\right) - \frac{1}{\hat{\lambda}_u}\tilde{\phi}_u\dot{\hat{\phi}}_u - \frac{1}{\hat{\lambda}_r}\tilde{\phi}_r\dot{\hat{\phi}}_r + \sigma_u\left(\tau_{wu}^* - \hat{\tau}_{wu}^*\right)\left(\hat{\tau}_{wu}^* - \tau_{wu}^0\right). \tag{46}$$

$$+ \sigma_r\left(\tau_{wr}^* - \hat{\tau}_{wr}^*\right)\left(\hat{\tau}_{wr}^* - \tau_{wr}^0\right) + Z_u S_u + Z_r S_r + \dot{\eta}$$

From Young's inequality, we have the following inequalities:

$$2S_u\phi_u^{*\mathrm{T}}h \le S_u^2\left\|\phi_u^*\right\|^2\|h\|^2 + 1 = S_u^2\phi_u h^{\mathrm{T}}h + 1,\ 2S_r\phi_r^{*\mathrm{T}}h \le S_r^2\left\|\phi_r^*\right\|^2\|h\|^2 + 1 = S_r^2\phi_r h^{\mathrm{T}}h + 1$$

$$- \sigma_u\tilde{\tau}_{wu}^*\left(\tilde{\tau}_{wu}^* - \tau_{wu}^0\right) \le -\frac{\sigma_u}{2}\tilde{\tau}_{wu}^* + \frac{\sigma_u}{2}\left(\tau_{wu}^* - \tau_{wu}^0\right)^2 - \sigma_r\tilde{\tau}_{wr}^*\left(\tilde{\tau}_{wr}^* - \tau_{wr}^0\right) \le -\frac{\sigma_r}{2}\tilde{\tau}_{wr}^* + \frac{\sigma_r}{2}\left(\tau_{wr}^* - \tau_{wr}^0\right)^2. \tag{47}$$

Then, we have the following inequalities

$$\dot{V} \le -\eta_1 s_1^2 - \eta_2 s_2^2 + \frac{1}{2}s_1^2\tilde{\phi}_1 h^{\mathrm{T}}h + \frac{1}{2}s_2^2\tilde{\phi}_2 h^{\mathrm{T}}h + \frac{\zeta_U^2}{2} + \frac{s_1^2}{2} + \frac{\zeta_R^2}{2} + \frac{s_2^2}{2} - \frac{1}{\hat{\lambda}_1}\tilde{\phi}_1\dot{\hat{\phi}}_1 - \frac{1}{\hat{\lambda}_2}\tilde{\phi}_2\dot{\hat{\phi}}_2 + 0.2785\varepsilon_1\tau_{\mathbf{wu}}^* + 0.2785\varepsilon_2\tau_{\mathbf{wr}}^*$$

$$- \frac{\sigma_1}{2}\left(\hat{\tau}_{\mathbf{wu}}^* - \tau_{\mathbf{wu}}^0\right)^2 + \frac{\sigma_1}{2}\left(\tau_{wu}^* - \tau_{wu}^0\right)^2 - \frac{\sigma_2}{2}\left(\hat{\tau}_{wr}^* - \tau_{wr}^0\right)^2 + \frac{\sigma_2}{2}\left(\tau_{wr}^* - \tau_{wr}^0\right)^2 + 1$$

$$= -\frac{2\eta_1 - 1}{2}s_1^2 - \frac{2\eta_2 - 1}{2}s_2^2 - \frac{\sigma_1}{2}\left(\hat{\tau}_{\mathbf{wu}}^* - \tau_{wu}^*\right)^2 - \frac{\sigma_2}{2}\left(\hat{\tau}_{wr}^* - \tau_{wr}^*\right)^2 + \tilde{\boldsymbol{\phi}}_1\left(\frac{1}{2}s_1^2\boldsymbol{h}^{\mathrm{T}}\boldsymbol{h} - \frac{1}{\hat{\lambda}_1}\dot{\hat{\boldsymbol{\phi}}}_1\right) + \tilde{\boldsymbol{\phi}}_2\left(\frac{1}{2}s_2^2\boldsymbol{h}^{\mathrm{T}}\boldsymbol{h} - \frac{1}{\hat{\lambda}_2}\dot{\hat{\boldsymbol{\phi}}}_2\right)$$

$$+ 0.2785\varepsilon_1\dot{\tau}_{wu} + 0.2785\varepsilon_2\dot{\tau}_{wr} + \frac{\zeta_U^2}{2} + \frac{\zeta_R^2}{2} + \frac{\sigma_1}{2}\left(\tau_{wu}^* - \tau_{wu}^0\right)^2 + \frac{\sigma_2}{2}\left(\tau_{wr}^* - \tau_{wr}^0\right)^2 + \frac{N_u^2}{4\alpha_1} + 1$$

$$= -\frac{2\eta_1 - 1}{2}s_1^2 - \frac{2\eta_2 - 1}{2}s_2^2 - \left(\frac{1}{T} - \alpha_1\right)y_1^2 - \frac{\sigma_1}{2}\left(\hat{\tau}_{wu}^* - \tau_{wu}^*\right)^2 - \frac{\sigma_2}{2}\left(\hat{\tau}_{wr}^* - \tau_{wr}^*\right)^2 + \kappa_1\tilde{\phi}_1\hat{\phi}_1 + \kappa_2\tilde{\phi}_2\hat{\phi}_2 + 0.2785\varepsilon_1\tau_{wu}^*$$

$$+ 0.2785\varepsilon_2\tau_{wr}^* + \frac{\zeta_U^2}{2} + \frac{\zeta_R^2}{2} + \frac{\sigma_1}{2}\left(\tau_{wu}^* - \tau_{wu}^0\right)^2 + \sigma_2\left(\tau_{wr}^* - \hat{\tau}_{wr}^*\right)\left(\hat{\tau}_{wr}^* - \tau_{wr}^0\right) - \frac{1}{\hat{\lambda}_1}\tilde{\phi}_1\dot{\hat{\phi}}_1 - \frac{1}{\hat{\lambda}_2}\tilde{\phi}_2\dot{\hat{\phi}}_2 \tag{48}$$

$\tilde{\phi}_1\hat{\phi}_1$ and $\tilde{\phi}_2\hat{\phi}_2$ satisfy the following inequality

$$2\tilde{\phi}_1\hat{\phi}_1 = \phi_1^2 - \hat{\phi}_1^2 - \tilde{\phi}_1^2 \le \phi_1^2 - \tilde{\phi}_1^2,\ 2\tilde{\phi}_2\hat{\phi}_2 = \phi_2^2 - \hat{\phi}_2^2 - \tilde{\phi}_2^2 \le \phi_2^2 - \tilde{\phi}_2^2. \tag{49}$$

Substituting Equation (49) into Equation (48) yields

$$\dot{V} = -\frac{2\eta_1 - 1}{2}s_1^2 - \frac{2\eta_2 - 1}{2}s_2^2 - \frac{\sigma_1}{2}\left(\hat{\tau}_{wu}^* - \hat{\tau}_{wu}^*\right)^2 - \frac{\sigma_2}{2}\left(\hat{\tau}_{wr}^* - \hat{\tau}_{wr}^*\right)^2 - \frac{\kappa_1}{2}\tilde{\phi}_1^2 - \frac{\kappa_2}{2}\tilde{\phi}_2^2 + 0.2785\varepsilon_1\tau_{wu}^*$$

$$+ 0.2785\varepsilon_2\tau_{wr}^* + \frac{\zeta_U^2}{2} + \frac{\zeta_R^2}{2} + \frac{\sigma_1}{2}\left(\tau_{wu}^* - \tau_{wu}^0\right)^2 + \frac{\sigma_2}{2}\left(\tau_{wr}^* - \tau_{wr}^0\right)^2 + \frac{N_u^2}{4\alpha_1} + 1 + \frac{\kappa_1}{2}\phi_1^2 + \frac{\kappa_2}{2}\phi_2^2 \tag{50}$$

Letting $V = V_0 + V_1$ and taking the derivative of V, we can get:

$$\dot{V} \le -C_1 V + C_2, \tag{51}$$

where $C_1 = min\left\{\frac{2\eta_1-1}{2}, \frac{2\eta_2-1}{2}, \frac{\sigma_1}{2}, \frac{\sigma_2}{2}, \frac{2\lambda_3-\beta\varepsilon^{\frac{2}{3}}-\beta\varepsilon^{\frac{2}{3}}\overline{B}}{\varepsilon\lambda_2}\right\}$ and $C_2 = 0.2785\varepsilon_1\tau^*_{wu}+0.2785\varepsilon_2\tau^*_{wr}+\frac{\xi^2_U}{2}+\frac{\xi^2_R}{2}+\frac{\sigma_1}{2}\left(\tau^*_{wu}-\tau^0_{wu}\right)^2+$

$\frac{\sigma_2}{2}\left(\tau^*_{wr}-\tau^0_{wr}\right)^2 + \frac{N^2_u}{4\alpha_1} + 1 + \frac{\kappa_1}{2}\phi^2_1 + \frac{\kappa_2}{2}\phi^2_2 + \frac{\varepsilon^{\frac{1}{3}}}{2}\beta(M^2+\overline{B})$. Solving Equation (51) gives

$$0 < V(t) \le (V(0) - \frac{C_2}{C_1})e^{-C_1 t} + \frac{C_2}{C_1}. \tag{52}$$

Based on Lemma 3, Equations (51) and (52), we conclude that $V(t)$ is uniformly ultimately bounded, which implies that all error signals S_u, S_r, $\widetilde{\phi}_u$, $\widetilde{\phi}_r$, $\widetilde{\tau}^*_u$ and $\widetilde{\tau}^*_r$ are ultimately uniformly bounded. Furthermore, since the error signals u_e and r_e are ultimately bounded, it follows that x_e and y_e are also bounded. By appropriately choosing the parameter $\frac{C_2}{C_1}$, it can be made arbitrarily small, ensuring that the tracking error becomes negligible, allowing the USV to track the trajectory with high accuracy.

Next, we first prove that there exists a Zeno-free phenomenon in the ETESO. By the definition of ETESO in Equation (6) and the definition of Equation ($\sigma(t)$), we can get

$$|y(t(o,k)) - y(t))| \le \frac{\overline{B}\varepsilon^3}{\sum^{i=1}_3 L_i}. \tag{53}$$

Then, for the error $\sigma(t)$ in Equation (6), as $t \in [t_{o,k}, t_{o,k+1})$, the following result $|y(t(o,k)) - y(t))| = \int^t_{t_{o,k}}|\dot{x}_1|d\tau = \int^t_{t_{o,k}}|x_2|d\tau$ holds. Since the system states are bounded, there exists $B > 0$ such that the inequality $|y(t(o,k)) - y(t))| = \int^t_{t_{o,k}}|x_2|d\tau \le (t-t(o,k))B$ holds. Therefore, for $t = t(o,k) + \check{\tau}$, there exists $\check{\tau} = \frac{\overline{B}\varepsilon^3}{B\sum^{i=1}_3 L_i}$ such that $y(t) - y(to,k) \le \frac{\overline{B}\varepsilon^3}{\sum^{i=1}_3}$. Accordingly, it comes to the result that the interval between $t_{0,k}$ and $t_{0,k+1}$ satisfies $\{t_{0,k+1} - t_{0,k}\} \ge \check{\tau} > 0$.

Finally, we prove that no Zeno phenomenon occurs by contradiction. Suppose that there exists Zeno phenomenon, then $\lim_{j\to\infty} t_j = T_0 < \infty$, where T_0 is a positive constant, and $\lim_{j\to\infty} \triangle j = 0$ with $\triangle j = t_{j+1} - t_j$. By the existence of the limit, for any constant $\epsilon_0 > 0$, there exists a positive integer $N(\epsilon_0)$, such that

$$t_j \in [T_0 - \epsilon_0, T_0], \forall \sigma > N(\epsilon_0). \tag{54}$$

Define the triggering instant as $\tau = t_{j+1}$. Note that once one event is triggered, then from Equation (29), the measurement error $Z(t)$ is reset to zero, that is, $||Z(\tau^+)|| = 0$. Just before the triggering, the following inequality can be obtained from Equation (30)

$$\eta_i(\tau^-) + (k_i - 1)S^2_i(\tau^-) - Z^2_i(\tau^-) \le 0, \tag{55}$$

it is easy to see that

$$\eta_i(\tau^-) \le Z^2_i(\tau^-), \tag{56}$$

there exists a constant $L_i > 0$, such that

$$Z^2_n(t) = \left(||Z(t_j) - Z(t)||\right)^2 \le L_i(t-t_j) \quad . \tag{57}$$

From Equations (56) and (57), we can have

$$L_i\Delta_j \ge Z^2_n(t^-_{j+1}) \ge \eta(t^-_{j+1}) \ge \frac{\eta_0 e^{-(\chi+\frac{1}{\lambda})t_{j+1}}}{\lambda} \ge \frac{\eta_0 e^{-(\chi+\frac{1}{\lambda})T_0}}{\lambda}, \tag{58}$$

It is easy to see by Equation (58) that when $\lim_{j\to\infty} t_j = T_0 < \infty$, the assumption about $\lim_{j\to\infty} \Delta_j = 0$ cannot be obtained, which results in a contradiction. Therefore, the Zeno phenomenon does not occur. Based on the above calculation, Theorem 1 is proved.
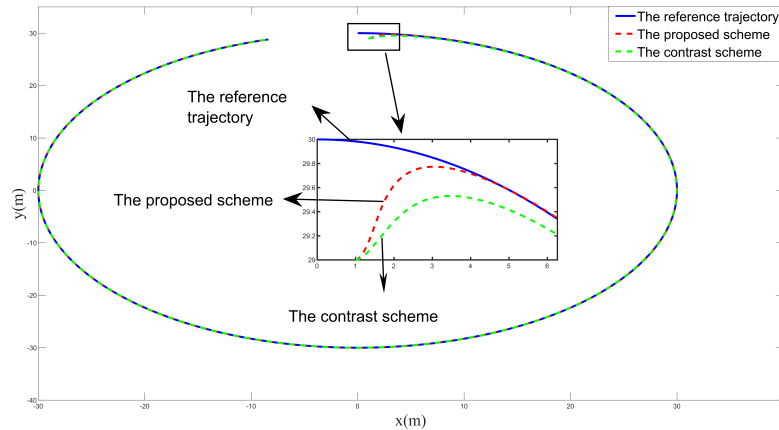
Figure 2. The reference and actual trajectories in the x-y plane.

5. SIMULATION ANALYSIS

To provide a more convincing demonstration of the effectiveness of the proposed trajectory tracking controller, the algorithm presented in this paper is compared with a commonly used event-triggered sliding mode algorithm based on LOS. The benchmark algorithm integrates the LOS guidance rate[38], event-triggered mechanism[26], linear sliding surface[28], and state observer extension[41]. In order to verify the effectiveness of the proposed unmanned boat tracking control strategy and formation control strategy, a model boat Cybership II USV developed by the Norwegian University of Science and Technology was selected for the simulation experimental study. The model mass m = 23.8 kg, length L_i = 1.225 m width B_i = 0.29 m, the center of gravity is at a distance x axis from the origin x_g = 0.046 m, and the inertia moment I_z = 0.046 m. The relevant model parameters are in ref.[42].

In the ETESO, $\alpha_i(\vartheta)$ is selected as α_1 = 3, $\alpha_2(\vartheta)$ = 3, α_3 = 1, L_1 = 3.25, L_2 = 3, L_3 = 1, $\overline{B}$ = 10, ε_e = 0.1 We set the reference trajectory as x_d = $300sin(0.03t)$ and y_d = $300cos(0.03t)$. The initial position of the USV is $x(0)$=1 m, $y(0)$=29 m, $\psi(0)$=0 rad, $u(0)$=0 m/s, $v(0)$=0 m/s and $r(0)$=0 rad/s. The control parameters are k_u = 10, k_r = 10, λ_u = 10, λ_r = 10 , β_u = 1.5, β_r = 1.5, r_u = 1.1, r_r = 1.2. Parameters of adaptive laws are τ_{wu}^0 = 0.1, τ_{wr}^0 = 0.1, γ_u = 12, γ_r = 12, Parameters of update laws are $\hat{\lambda}_u$ = 10 and $\hat{\lambda}_r$ = 10. To testify to the robustness and effectiveness of the proposed controller, the disturbances are assumed to be as follows: $\Delta f_u = 0.5 + 0.25 \sin(0.01t)$, $\Delta f_r = -40 + 2.5 \cos(0.10t)$. $\tau_{wu} = \sin(0.2t) + \cos(0.5t)$, $\tau_{wr} = \sin(0.5t) + \cos(0.3t)$. The time-varying target trajectory is chosen as follows:

$$\begin{bmatrix} x_d \\ y_d \end{bmatrix} = \begin{bmatrix} 30sin(0.03t) \\ -40 + 2.5cos(0.03t) \end{bmatrix}. \tag{59}$$

The numerical results are shown in Figures 2-8. Figure 2 shows the trajectory tracking comparison simulation results between the proposed algorithm and the control algorithm under model uncertainty and external disturbances. The experimental results indicate that both controllers can accurately track the desired trajectory. However, the proposed solution demonstrates better performance in terms of convergence speed during the initial control phase. Meanwhile, the corresponding tracking error is shown in Figure 3, which indicates that the USV can track the reference position within approximately six seconds and achieve faster error stabilization compared to the control scheme. Figure 4 compares the velocity tracking results between the proposed algorithm and the control algorithm. From the zoomed-in view of the components, it can be seen that both the proposed algorithm and the control algorithm can track the velocity well, but the proposed algorithm
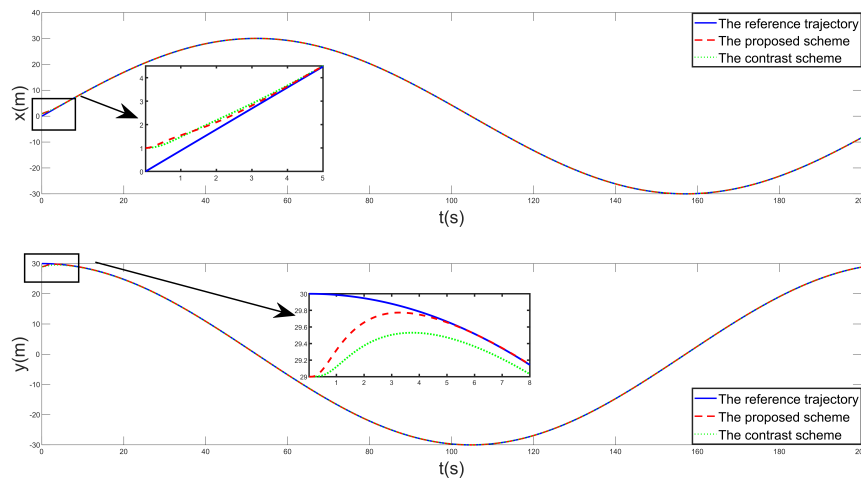
Figure 3. The curves of reference and actual positions.
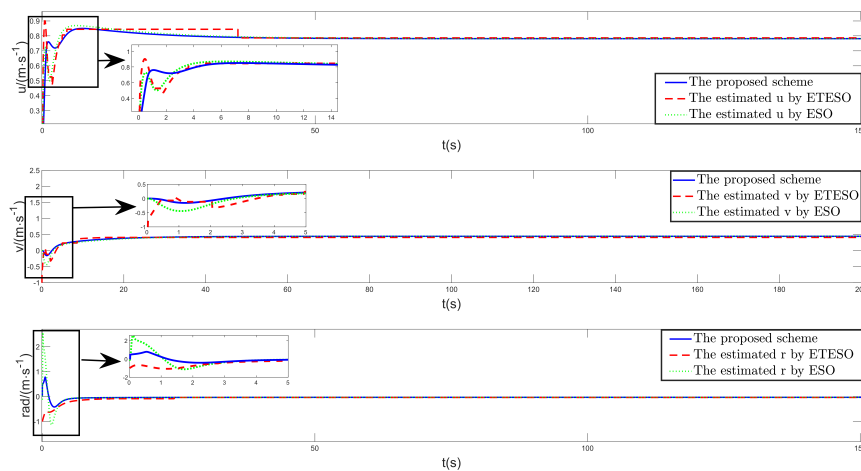

Figure 4. The comparison of actual and estimated velocities in the ETESO. ETESO: Event-triggered extended state observer.

requires fewer trigger occurrences. The control inputs τ_u and τ_r are shown in Figure 5. It can be observed that, compared to the control scheme, the proposed scheme exhibits smaller fluctuations in the control signals. As shown in Figure 6, the model uncertainty of USVs can be accurately estimated and approximated using MLP neural networks. According to the above simulation results, it can be concluded that the proposed controller has faster convergence and better robustness. Figure 7 shows the estimation of the lumped disturbance. Therefore, both the proposed and contrast algorithms can observe and estimate the unmeasurable velocity and lumped disturbance with minimal error, demonstrating excellent estimation performance. Figure 8 shows that the adaptive law can estimate the upper bound of the external disturbance by selecting the appropriate parameters. Figure 9 shows triggering instants and triggering time of τ_u, τ_r and ETESO. It is clear that, compared to the static event-triggering mechanism in the comparative experiments, the DETM used in the proposed algorithm results in longer intervals between controller-triggered events.
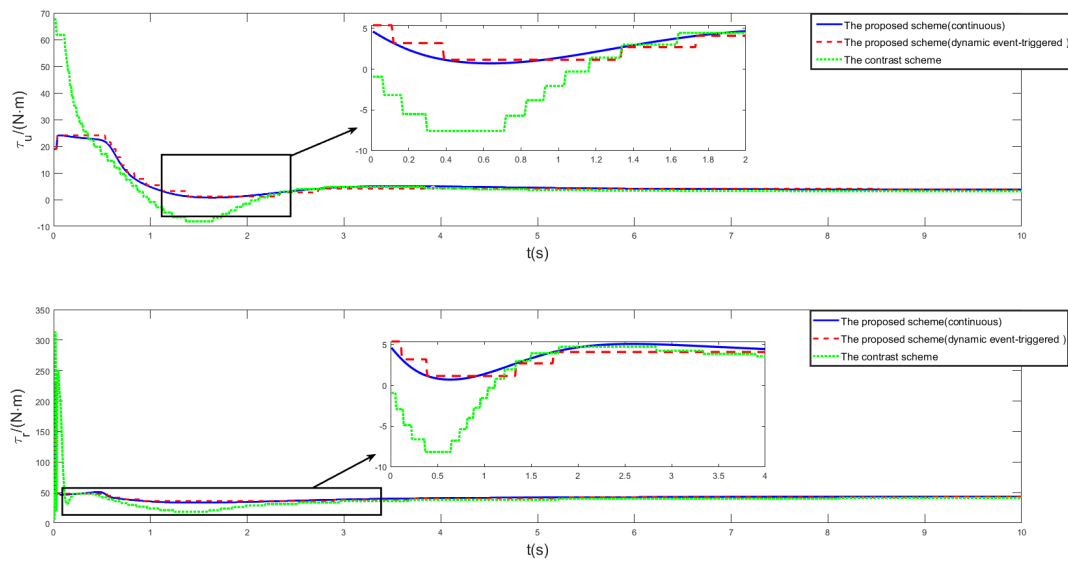
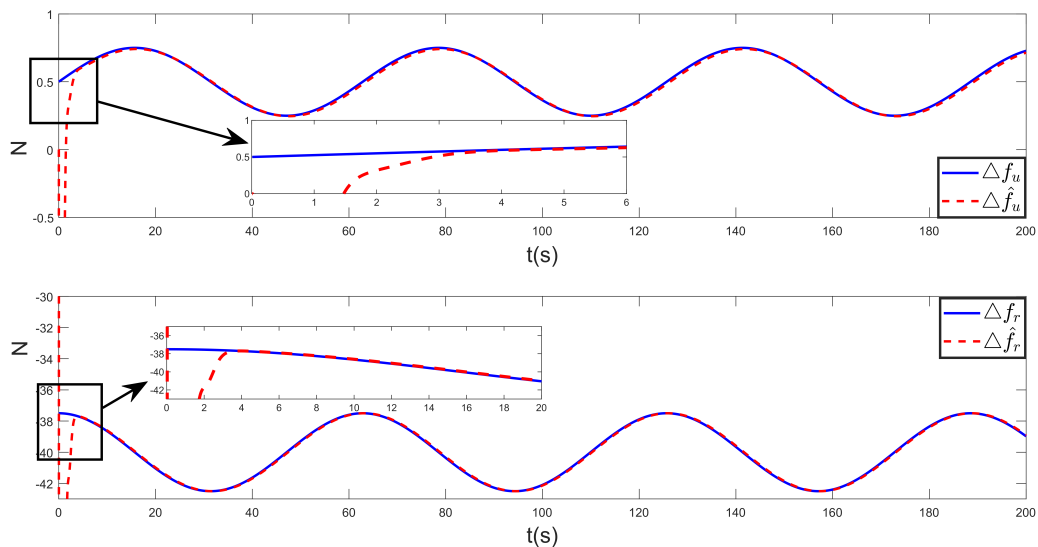**Figure 5.** Controller inputs τ_u and τ_r.

Figure 6. The model uncertainty curves approximated by MLP. MLP: Minimum learning parameter.

6. CONCLUSION

Based on the nonlinear mathematical model with model uncertainties and external disturbances, a INTSM control method based on DETM is proposed. This approach integrates ETESO, NTSM, DETM, MLP neural networks, and adaptive techniques. To address the issue of difficult-to-measure velocity in practical applications, an ETESO is designed to accurately estimate the unmeasurable velocity and lumped disturbances. To improve the system's convergence speed and reduce steady-state error, INTSM is used to design the control input. Additionally, a DETM is incorporated into the controller, considering communication and actuator wear issues in the USV. To enhance the robustness of the control system, an MLP technique is employed to
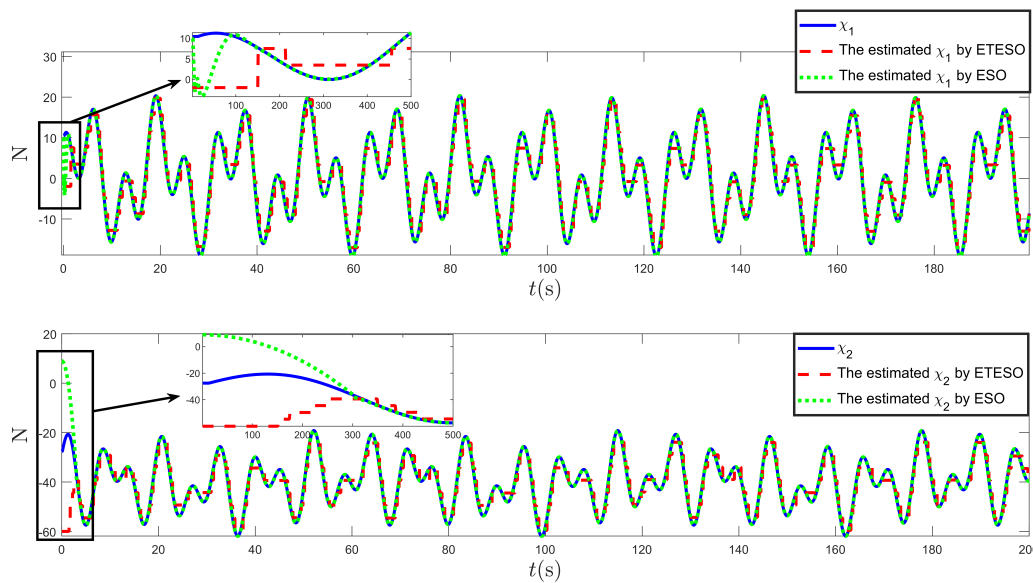
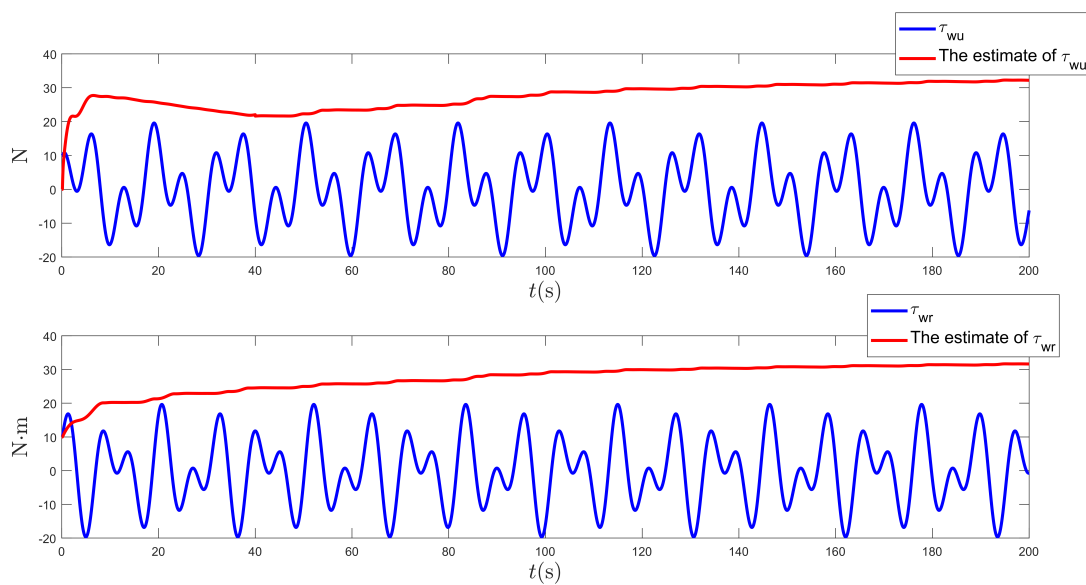**Figure 7.** The lumped disturbances and observer estimations.

Figure 8. The external disturbances and their boundary estimations.

approximate and compensate for model uncertainties. An adaptive law is also designed to compensate for the neural network approximation errors and disturbances. Furthermore, through rigorous theoretical analysis, the overall stability of the closed-loop control system is proved, and it is demonstrated that the tracking error converges to a small neighborhood of the origin. Finally, comparative numerical simulations are conducted to analyze the tracking performance. The simulation results fully demonstrate the effectiveness and superiority of the proposed approach. In the future, to further conserve communication resources, we will consider replacing the event-triggered mechanism in ETESO with a DETM and verifying the proposed algorithm in practical applications.
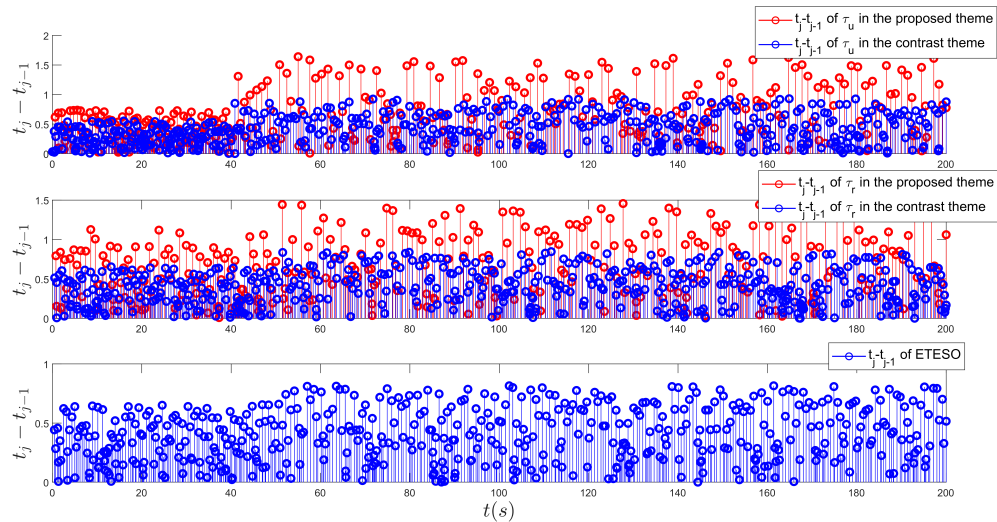
Figure 9. Triggering instants and triggering time of τ_u, τ_r and ETESO. ETESO: Event-triggered extended state observer.

DECLARATIONS

Authors' contributions

Conceptualization, methodology, manuscript writing and technical support: Wang X

Data acquisition: Liu R

Reviewing and editing: Li Q, Aleksander S

Supervision: Jiang R

Availability of data and materials

The data that support the findings of this study are available from the corresponding author upon reasonable request.

Conflicts of interest

All authors declared that there are no conflicts of interest.

Ethical approval and consent to participate

Not applicable.

Consent for publication

Not applicable.

REFERENCES

1. Liu Z, Zhang Y, Yu X, Yuan C. Unmanned surface vehicles: an overview of developments and challenges. *Annu Rev Control* 2016;41:71–93. DOI

2. Su M, Pu R, Wang Y, Yu M. A collaborative siege method of multiple unmanned vehicles based on reinforcement learning. *Intell Robot* 2024;4:39–60. DOI

3. Barrera C, Padrón Armas I, Luis F, Llinas O, Marichal Plasencia GN. Trends and challenges in unmanned surface vehicles (USV): from survey to shipping. *TransNav* 2021;15:135–42. DOI

4. Xue K, Liu J, Xiao N, Ji X, Qian H. A bio-inspired simultaneous surface and underwater risk assessment method based on stereo vision for USVs in nearshore clean waters. *IEEE Robot Autom Lett* 2023;8:360–7. DOI

5. Zhao L, Bai Y. Unlocking the ocean 6G: a review of path-planning techniques for maritime data harvesting assisted by autonomous marine vehicles. *J Mar Sci Eng* 2024;12:126. DOI

6. Zhang G, Liu S, Huang J, Zhang W. Dynamic event-triggered path-following control of underactuated surface vehicle with the experiment verification. *IEEE T Veh Technol* 2022;71:10415–25. DOI

7. Wang YL, Han QL. Network-based fault detection filter and controller coordinated design for unmanned surface vehicles in network environments. *IEEE Trans Ind Informat* 2016;12:1753–65. DOI

8. Wang X, Fei Z, Gao H, Yu J. Integral-based event-triggered fault detection filter design for unmanned surface vehicles. *IEEE Trans Ind Informat* 2019;15:5626–36. DOI

9. Jiang C, Zhang G, Huang C, Zhang W. Memory-based event-triggered path-following control for a USV in the presence of DoS attack. *Ocean Eng* 2024;310:118627. DOI

10. Zhou L, Shen Z, Nie Y, Yu H. Event-triggered adaptive dynamic programming for optimal tracking control of unmanned surface vessel with input constraints. *Trans Inst Meas Control* 2023 NOV;45:2835–47. DOI

11. Girard A. Dynamic triggering mechanisms for event-triggered control. *IEEE Trans Autom Control* 2015 ;60:1992–7. DOI

12. Cao L, Yao D, Li H, Meng W, Lu R. Fuzzy-based dynamic event triggering formation control for nonstrict-feedback nonlinear MASs. *Fuzzy Set Syst* 2023;452:1–22. DOI

13. He W, Xu B, Han QL, Qian F. Adaptive consensus control of linear multiagent systems with dynamic event-triggered strategies. *IEEE Trans Cybern* 2020;50:2996–3008. DOI

14. Wang XY, Chang XH. Nonlinear continuous-time system H∞ control based on dynamic quantization and event-triggered mechanism. *Neural Proc Lett* 2023;55:12223–38. DOI

15. Alfaro-Cid E, McGookin EW, Murray-Smith DJ, Fossen TI. Genetic algorithms optimisation of decoupled Sliding Mode controllers: simulated and real results. *Control Eng Pract* 2005;13:739–48. DOI

16. Zhang Y, McEwen RS, Ryan JP, Bellingham JG. Design and tests of an adaptive triggering method for capturing peak samples in a thin phytoplankton layer by an autonomous underwater vehicle. *IEEE J Oceanic Eng* 2010;35:785–96. DOI

17. Rodriguez J, Castañeda H, Gonzalez-Garcia A, Gordillo JL. Finite-time control for an unmanned surface vehicle based on adaptive sliding mode strategy. *Ocean Eng* 202215;254:111255. DOI

18. Liu W, Ye H, Yang X. Super-twisting sliding mode control for the trajectory tracking of underactuated USVs with disturbances. *J Mar Sci Eng* 2023;11:636. DOI

19. Yu XN, Hao LY. Integral sliding mode fault tolerant control for unmanned surface vessels with quantization: less iterations. *Ocean Eng* 2022;260:111820. DOI

20. Zhang Q, Zhang S, Liu Y, Zhang Y, Hu Y. Adaptive terminal sliding mode control for USV-ROVs formation under deceptive attacks. *Front Mar Sci* 2024;11:1320361. DOI

21. Sun Q, Liu ZW, Chi M, Ge MF, He D. Robust coverage control of multiple USVs with time- varying disturbances. *Intell Robot* 2023;3:242–56. DOI

22. Han J, Xiong J, He Y, Gu F, Li D. Nonlinear modeling for a water-jet propulsion USV: an experimental study. *IEEE Trans Ind Electron* 2017;64:3348–58. DOI

23. Chen Z, Zhang Y, Zhang Y, Nie Y, Tang J, Zhu S. Disturbance-observer-based sliding mode control design for nonlinear unmanned surface vessel with uncertainties. *IEEE Access* 2019;7:148522–30. DOI

24. Chen Z, Zhang Y, Nie Y, Tang J, Zhu S. Adaptive sliding mode control design for nonlinear unmanned surface vessel using RBFNN and disturbance-observer. *IEEE Access* 2020;8:45457–67. DOI

25. Chang XH, Han X. Observer-based fuzzy $l_2 - l_\infty$ control for discrete-time nonlinear systems. *IEEE Trans Fuzzy Syst* 2024;32:2523–8. DOI

26. Ning J, Ma Y, Li T, Chen CLP, Tong S. Event-triggered based trajectory tracking control of under-actuated unmanned surface vehicle with state and input quantization. *IEEE Trans Intell Veh* 2024;9:3127–39. DOI

27. Wang H, Zhang S. Event-triggered reset trajectory tracking control for unmanned surface vessel system. In: Proceedings of the Institution of Mechanical Engineers, Part I: Journal of Systems and Control Engineering. 2021;235:633–45. DOI

28. Zhao Y, Sun X, Wang G, Fan h. Adaptive backstepping sliding mode tracking control for underactuated unmanned surface vehicle with disturbances and input saturation. *IEEE Access* 2021;9:1304–12. DOI

29. Zhu F, Peng Y, Cheng M, Luo J, Wang Y. Finite-time observer-based trajectory tracking control of underactuated USVs using hierarchical non-singular terminal sliding mode. *Cyber Phys Syst* 2022;8:263–85. DOI

30. Wan L, Su Y, Zhang H, Tang Y, Shi B. Global fast terminal sliding mode control based on radial basis function neural network for course keeping of unmanned surface vehicle. *Int J Adv Robot Syst* 2019;16:1729881419829961. DOI

31. Zhao C, Yan H, Gao D, Wang R, Li Q. Adaptive neural network iterative sliding mode course tracking control for unmanned surface

vessels. *J Math* 2022;2022:1417704. DOI

32. Bateman A, Hull J, Lin Z. A backstepping-based low-and-high gain design for marine vehicles. *Int J Robust Nonlinear Control* 2009;19:480–93. DOI

33. Zhang J, Liu X, Wang X, Wang Y, Wang Y. Adaptive prescribed performance tracking control for underactuated unmanned surface ships with input quantization. *Intell Robot* 2024;4:146–63. DOI

34. Huang T, Xue Y, Xue Z, Zhang Z, Miao Z, Liu Y. USV-tracker: a novel USV tracking system for surface investigation with limited resources. *Ocean Eng* 2024;312:119196. DOI

35. Qiu B, Wang G, Fan Y, Mu D, Sun X. Adaptive sliding mode trajectory tracking control for unmanned surface vehicle with modeling uncertainties and input saturation. *Appl Sci* 2019;9:1240. DOI

36. Li J, Zhang G, Li B. Robust adaptive neural cooperative control for the USV-UAV based on the LVS-LVA guidance principle. *J Mar Sci Eng* 2022;10:51. DOI

37. Wu GX, Ding Y, Tahsin T, Atilla I. Adaptive neural network and extended state observer-based non-singular terminal sliding modetracking control for an underactuated USV with unknown uncertainties. *Appl Ocean Res* 2023;135:103560. DOI

38. Yu S, Lu J, Zhu G, Yang S. Event-triggered finite-time tracking control of underactuated MSVs based on neural network disturbance observer. *Ocean Eng* 2022;253:111169. DOI

39. Guo BZ, Zhao Zl. On the convergence of an extended state observer for nonlinear systems with uncertainty. *Syst Control Lett* 2011;60:420–30. DOI

40. Huang Y, Wang J, Shi D, Shi L. Toward event-triggered extended state observer. *IEEE Trans Autom Control* 2018;63:1842–49. DOI

41. Xu Z, Xie N, Shen H, Hu X, Liu Q. Extended state observer-based adaptive prescribed performance control for a class of nonlinear systems with full-state constraints and uncertainties. *Nonlinear Dynam* 2021;105:345–58. DOI

42. Skjetne R, Fossen TI, Kokotović PV. Adaptive maneuvering, with experiments, for a model ship in a marine control laboratory. *Automatica* 2005;41:289–98. DOI